Periodico di Mineralogia (2013), 82, 2, 299-312 DOI: 10.2451/2013PM0018

PERIODICO di MINERALOGIA
established in 1930

An International Journal of
MINERALOGY, CRYSTALLOGRAPHY, GEOCHEMISTRY, ORE DEPOSITS, PETROLOGY, VOLCANOLOGY
and applied topics on *Environment*, *Archaeometry* and *Cultural Heritage*

Preliminary results of the spectroscopic and structural characterization of mesothelioma inducing crocidolite fibers injected in mice

Alessandro Francesco Gualtieri[1], Carlotta Giacobbe[2], Caterina Rinaudo[3,*], Alessandro Croce[3], Mario Allegrina[3], Giovanni Gaudino[4], Haining Yang[4] and Michele Carbone[4]

[1] Dipartimento di Scienze Chimiche e Geologiche, Università di Modena e Reggio Emilia, Italy
[2] Dipartimento di Scienze e Alta Tecnologia, Università dell'Insubria, Como, Italy
[3] Department of Science and Technological Innovation,
Università del Piemonte Orientale "Amedeo Avogadro", Alessandria, Italy
[4] University of Hawai'i Cancer Center - University of Hawai'i, USA and Department of Pathology,
John A. Burns School of Medicine - University of Hawai'i, HI 96813, USA
[*]Corresponding author: *caterina.rinaudo@mfn.unipmn.it*

Abstract

To investigate the structure and microstructure changes of crocidolite asbestos incorporated in biological tissues, fibers of this mineral phase were injected in mice peritoneum. Histological sections of different organs of mice developing mesothelioma after crocidolite inoculation were prepared and analysed by optical microscopy. The tumours developed within the peritoneal cavity, wrapped around the surrounding organs. Many fibers were observed in the fibrotic areas of the peritoneum lining pancreas and spleen. The raw fibers before inoculation and those embedded in mice tissues were characterized using Micro-Raman spectroscopy and in situ synchrotron X-ray diffraction at ESRF- Grenoble. Preliminary results indicate shifts of some bands on the Raman spectra and enlargement of the X-Ray diffraction peaks of the fibers localized in the mice tissue sections. A preliminary structural picture of the fibers incorporated in mice tissues suggests inter-crystalline migration of the iron and sodium ions.

Key words: Raman spectroscopy; Synchrotron diffraction; Rietveld method; crocidolite; asbestos; mesothelioma.

Introduction

As demonstrated by many scientific works, crocidolite is an asbestos phase responsible of the development of mesothelioma (MM), a deadly cancer characterized by the transformation of mesothelial cells (HM) lining the pleural, peritoneal or pericardial cavities (Aust et al.,

2011; Carbone et al., 2012; Case, 2011; De Vuyst et al., 1997; Fubini and Mollo, 1995; Goodglick and Kane, 1990; Huang et al., 2011; Koerten et al., 1990; Mossman et al., 1983; Tannapfel, 2011; Wagner et al., 1984; Werner et al., 1995; Yao et al., 2010; Zucali et al., 2011). Although many scientific papers were addressed to understand the mechanisms of interaction between the cells and the mineral fibers causing the pathogenicity of this mineral (see for example: Cole et al., 1991; Fubini and Mollo, 1995; Guthrie, 1992; Huang et al., 2011; Mossman et al., 1983; Rihn et al., 2000; Yang et al., 2010), the issue is still debated. Different approaches to the problem are possible: one may be to investigate the chemical and biochemical response of the cells and extracellular microenvironment to the mineral fibers (Bernstein et al., 2005; Brody, 1993; Guthrie, 1992; Mastrangelo et al., 2011; Toyokuni, 2009); another possible approach is the one used in this study: the analysis of the chemical-crystallographic changes of the fibers induced by the prolonged permanence inside the biological milieu. The characterization of fibers and inorganic phases in histological sections of lung and pleural plaque of patients affected by MM has been carried out by our research group using micro-Raman spectroscopy and the results were described in previous works (Croce et al., 2013a; Musa et al., 2012; Rinaudo et al., 2010a, b). It has also been demonstrated that micro-Raman analysis may be performed directly on the sections prepared for routine diagnostic purpose with no additional modifications. Notwithstanding, the latency time for the development of mesothelioma in humans may be very long and medical treatments may be a confounding element influencing the persistence of the respired fibers. To better understand the structure-microstructure changes of fibers induced by the contact with the tissues in situ, in this work we have attempted a combined spectroscopic and diffraction study of the standard UICC crocidolite fibers, injected in mice. In these animals MM developed in the peritoneal cavity and histological sections of the different surrounding organs were prepared. With the aid of an optical microscope crocidolite fibers were identified. Such fibers were therefore characterized by micro-Raman spectroscopy and Rietveld structure refinement, by use of data collected in situ at ESRF (Grenoble, France).

We describe here preliminary results on crocidolite fibers observed at the peritoneal surface adjacent to pancreas and spleen, where they appear free or coated by ferruginous material, forming the well-known “asbestos bodies” or “ferruginous bodies” (Arul and Holt, 1980; Croce et al., 2013b; Dodson et al., 1993; Gellert et al., 1986; Ghio et al., 2004; Langer et al., 1972; Pascolo et al., 2011; Sakai et al., 2010). To highlight variation in structural-spectroscopic characteristics after permanence in the mice tissues, raw fibers of the powder used for injection are characterized using the two techniques under the same experimental conditions.

Materials and methods

Fifteen BALB/c mice were injected intra-peritoneum (i.p.) using crocidolite purchased from UICC (Union for International Cancer Control) at the University of Hawai’i Cancer Center. A total amount of 4 mg was subdivided in 10 doses and given every two weeks in 50 µl PBS. During the following 28 months, animals were euthanized when they developed ascites. Formalin-fixed, Paraffin Embedded (FFPE) tissue sections of the different organs were prepared to identify the presence of mineral fibers with optical microscopy. In this preliminary work, FFPE tissue sections from pancreas and spleen were analysed. In order to avoid Raman band interference with those produced by the inorganic fiber, unstained FFPE sections were analyzed. The spectroscopic study was carried out using a Jobin Yvon HR800

LabRam μ-spectrometer, equipped with an Olympus BX41 microscope on which a rotating plate with vernier was mounted, a HeNe 20 mW laser working at 632.8 nm and a charge-coupled device (CCD) air-cooled detector. Instrument calibration was carried out before each analysis, by checking the position and intensity of the Si band at 520.65 ± 0.05 cm^{-1}. To balance signal against noise, 100 cycles of 100 s (about 11 h) were performed. The spectral region recorded ranged from 1200 cm^{-1} to 200 cm^{-1}, where vibrational lattice modes in the asbestos occur (Foresti et al., 2009; Fornero et al., 2008; Giacobbe et al., 2010; Rinaudo et al., 2003, 2004, 2005). A confocal hole fixed at 200 μm allowed to record spectra with well-defined Raman bands. To enhance the differences in the relative intensities of the Raman bands in fibers after a period in the mice biological system, all the fibers were placed with the same orientation and precisely with their elongation axis exactly at 45° with respect to the N-S direction of the cross-hair of the microscope, annexed to the spectrometer. All the Raman spectra were recorded keeping the experimental conditions fixed. The recorded spectra were processed using ORIGIN software v 6.0.

The chemical characterization of the fibers was performed under VP-SEM/EDS, using an E-SEM Quanta 200 model of the FEI group, equipped with EDS detector of EDAX system. This allows sample characterization on unpolished coating-free samples. The analyses were carried out under a pressure value of 90 Pa and 20 kV as the accelerating voltage. The registered spectra were processed using the GENESIS software v 3.6.

Tentative structural characterization of the raw crocidolite fibers and of those inoculated in the peritoneum and detected around the spleen and pancreas was attempted to verify the structure changes induced by the interaction of the crocidolite fibers with the organic matrix. The in situ experimental data were collected at BM01 beamline at ESRF facility, using an X-ray beam of 100x100 μm. The organic tissues inoculated with the fibers were prepared on plastic substrates, sometimes glued with paraffin, and fixed by a thin kapton foil. Data were collected with a 200 mm sample to detector distance, a wavelength of 0.75276 Å on the MARR CCD two-dimensional detector with a 360 s exposure time and a 2300x2300 pixel area. Data reduction of the two dimensional pictures to obtain powder patterns was done using the FIT2D (Hammersley et al., 1996) software. All the collected powder patterns show broad peaks from the components used for the sample preparation (kapton, plastic and paraffin), which severely overlap with crocidolite peaks. Notwithstanding, differences in the peak intensity of the raw sample with respect to the fibers inoculated in the organic media were detected.

The Rietveld structure refinements were performed using GSAS (Larson and Von Dreele, 1994) and its graphical interface EXPGUI (Toby, 2001). For all the data sets, the pseudo-Voigt profile function coefficients GW (angle-independent term of the Gaussian broadening) and Lx (crystal size term of the lorentzian broadening) were refined together with the unit cell, scale factor and background shifted Chebyshev coefficients. Several excluded regions were considered to remove the peaks generated by the sample holder. This causes the loss of some crocidolite Bragg peaks, significantly reducing the accuracy of the results. For this reason, all the structure parameters (coordinates, site populations and overall adp's) were refined only for the starting raw crocidolite sample whereas only the site populations of the M and Am sites were refined in the spleen and pancreas crocidolite samples. The riebeckite structure calculated by Hawthorne (1978) was taken as initial model for crocidolite. For all the samples, magnesium was refined in the M1 position with a population kept fixed to the value

obtained from the ideal chemical composition (0.50 a.f.u.) taken from the literature (Kohyama et al., 1996).

Results and discussion

A morphological and chemical characterization of the raw crocidolite is shown in Figure 1: as expected EDS peaks from Si, Fe, Na and Mg are detected (Bowes and Farrow, 1997). At first, a thorough characterization of these raw crocidolite fibers was performed recording Raman spectra and placing, thanks to the rotating plate, the different fibers at the same orientation with respect to the laser beam direction. The Raman spectra were therefore summarized and the average for each Raman band calculated, obtaining the result shown in Figure 2. The Raman spectrum contains many bands, generated by the vibrations of the different coordination polyhedra forming the crystal structure (Burns and Prentice, 1968). The tetrahedral units (mainly Si-O bonds) are responsible for the intense bands in the spectrum. In particular the band at 1087 cm^{-1} may be ascribed to antisymmetric (ν_{as}) stretching vibrations of the Si-O_b-Si linkages, the band at 970 cm^{-1} to ν_s modes of O-Si-O bonds, the bands at 666, 579, 540 and 510 cm^{-1} to the symmetric stretching modes (ν_s) and to the deformation modes of Si_4O_{11} groups (Apopei and Buzgar, 2010; Bard et al., 1997; Lewis et al., 1996; Rinaudo et al., 2004). More complicated is the assignment of the bands in the spectral range 500-200 cm^{-1}, due to the vibrational modes of the cations in cubic or octahedral coordination, the bending modes of the Si-centred tetrahedra and in general all the lattice modes. In this spectral region, exact assignment of the different bands to the vibrational mode of a specific chemical group represents a challenge.

The optical analysis of the tissue sections from mice organs showed many crocidolite fibers in the fibrotic areas of the peritoneal surface of spleen and pancreas, as seen on Figure 3. As reported in literature, crocidolite fibers in the biological medium often appear coated by iron-protein material forming the well-known "ferruginous bodies" or "asbestos bodies" (Arul and Holt, 1980; Croce et al., 2013b; Dodson et al., 1993; Gellert et al., 1986; Ghio et al., 2004; Langer et al., 1972; Musa et al., 2012; Pascolo et al., 2011; Rinaudo et al., 2010b; Sakai et al., 2010). In the histological sections of mice tissues studied in the present work, the mechanism of fiber-coating occurred at different stages. At the

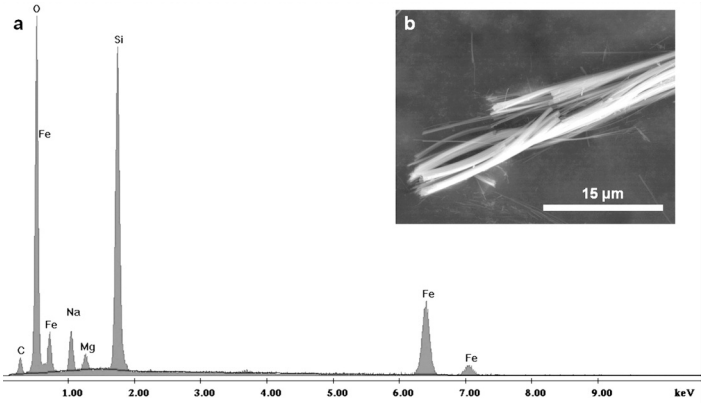

Figure 1. a) EDS spectrum of raw crocidolite sample used for injection in mice; b) SEM image of the bundle of crocidolite undergone to EDS spot analysis.

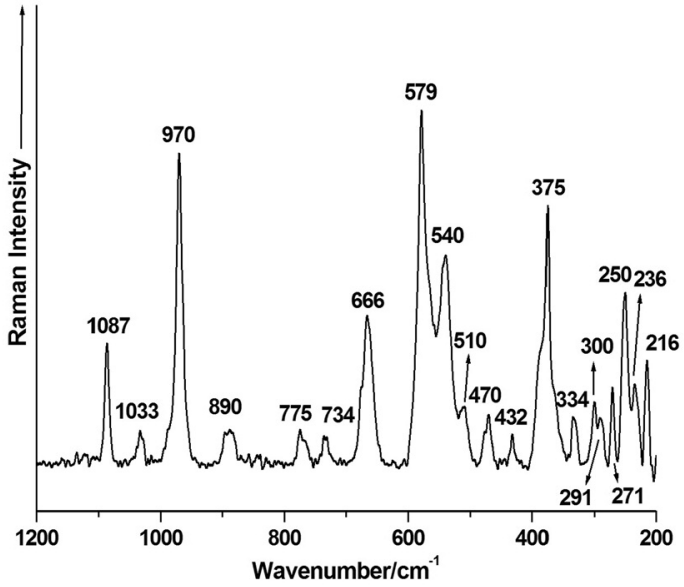

Figure 2. Raman spectrum of the raw crocidolite. The spectrum is obtained by merging the Raman spectra recorded on different fibres and hence calculating the mean value for each band.

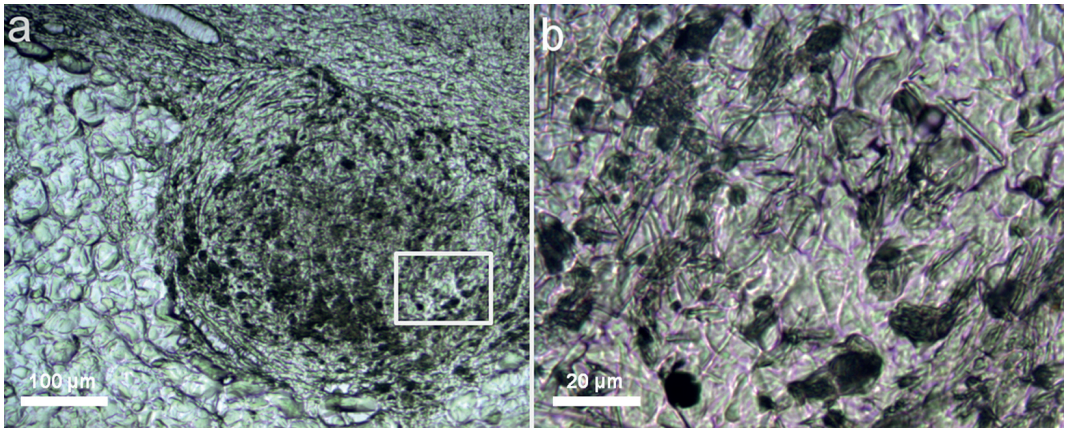

Figure 3. a) Optical photograph showing crocidolite fibres aggregated in the peritoneal surface of spleen; b) higher magnification of the area delimited in a).

beginning, the coating appears as a black film on the fiber (Figure 4a). In a further step, the characteristic features of the "asbestos bodies" are formed (Figure 4b). During this study only fibers free from coating, as that represented in Figure 4c, were selected for the Raman characterization. In this way, interference of the bands produced by the mineral phase with those generated by the coating was avoided. On several fibers observed at the surface of spleen, Raman spectra were recorded, all the spectra summarized and the average for each band calculated, obtaining the spectrum shown in Figure 5. Comparison with the spectrum in Figure 2 allows highlighting some differences:

- the band at 578 cm^{-1}, which appeared with intensity higher than that of the band at 970 cm^{-1} in raw crocidolite, exhibits now a lower intensity (Figure 2);
- the band near 375 cm^{-1} is asymmetric; the underlying components show different intensities, in particular the band at 363 cm^{-1} (Figure 5) appears more intense in the Raman spectra from fibers in mice;
- in the spectral region from 230 cm^{-1} to 250 cm^{-1}, shift of 4-5 cm^{-1} of the Raman bands of the fibers concentrated in spleen peritoneum is detected.

The fibers identified on the peritoneal surface of pancreas were analysed with the same experimental procedure. Often the Raman bands appeared with very low intensity. In other cases, good spectra could be recorded. Merging the spectra and calculating the average wavenumber for each band we obtained the result shown in Figure 6. In the 400-200 cm^{-1} region of the spectra, reduction in band signal from these fibers is observed. In particular, the band at 375 cm^{-1} shows reduced intensity and a component at 384 cm^{-1} appears. The band near 335 cm^{-1} splits in two components at 328 and 334 cm^{-1}.

In the Raman spectra of the crocidolite fibers in mice tissues, the vibrational modes of the Si-O bonds basically occur at the same wavenumbers as in raw crocidolite (Figures 2, 5 and 6). On the contrary, in the spectral region which displays the vibrational modes of the cations in the cubic or octahedral coordination shifts, splitting of bands or reduction of band intensity are evident. All these observations support a degradation or modification of the crystalline structure mainly affecting the cubic or octahedral polyhedra.

As far as the Rietveld structure refinements are concerned, the following agreement factors were obtained: (i) raw crocidolite fibers: background

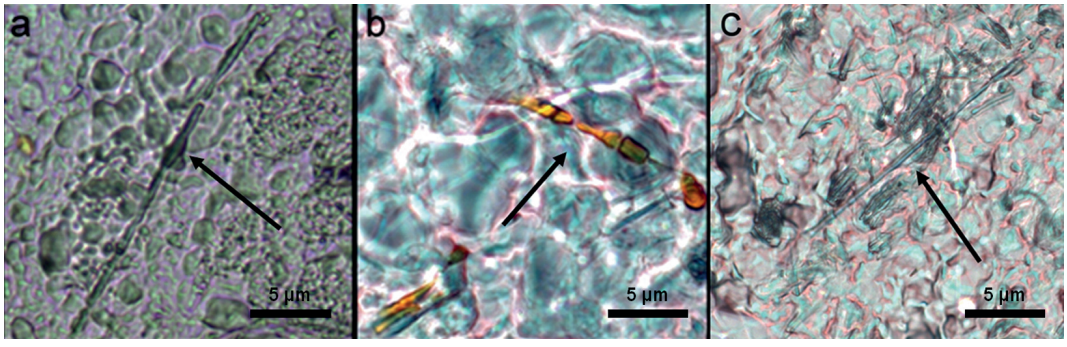

Figure 4. a) Optical photograph of a crocidolite fibre, showing the early step of the coating process (arrowed) in mice tissue; b) characteristic features of the "asbestos bodies", in a later advanced stage of the coating, arrowed; c) crocidolite fibre, free from coating- arrowed- selected for the Raman characterization.

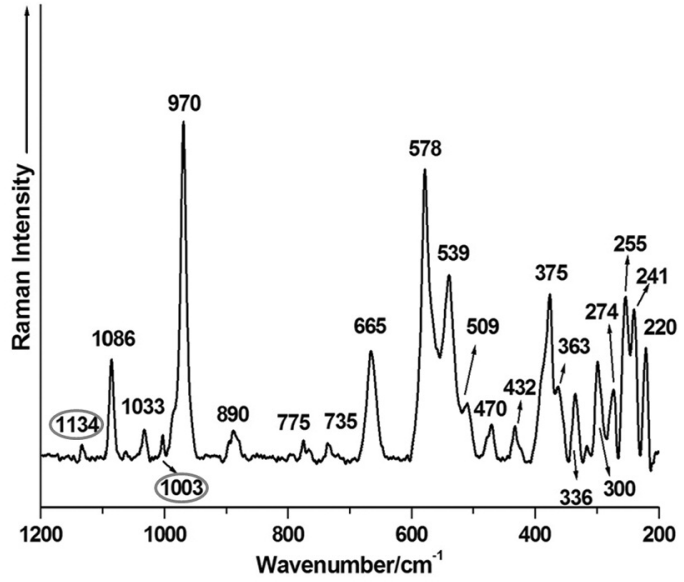

Figure 5. Raman spectrum of crocidolite fibres in spleen thin section. The spectrum is obtained by merging the Raman spectra recorded on different fibres and hence calculating the mean value for each band. Circled bands are produced by the paraffin film covering the thin section.

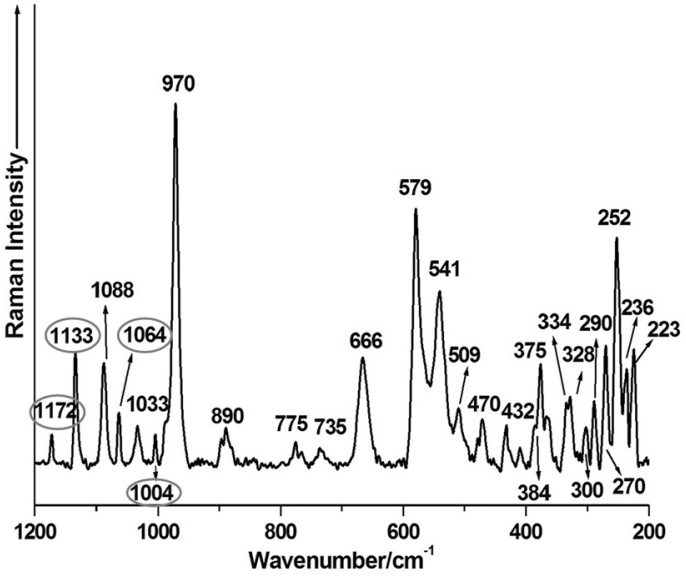

Figure 6. Raman spectrum of crocidolite fibres in pancreas thin section. The spectrum is obtained by merging the Raman spectra recorded on different fibres and hence calculating the mean value for each band. Circled bands are produced by the paraffin film covering the thin section.

Table 1. The structure parameters calculated from the Rietveld refinement of raw crocidolite.

site	x/a	y/b	z/c	Cation	Occ.	U_{iso}(Å^2)**
T1	0.2945(13)	0.0852(7)	0.3051(25)	Si	1.0	0.02245
T2	0.2731(14)	0.1704(7)	0.7946(29)	Si	1.0	0.02245
O1	0.1269(18)	0.0945(16)	0.232(6)	O	1.0	0.01695
O2	0.1047(19)	0.1764(14)	0.731(6)	O	1.0	0.01695
O-H3	0.106(4)	0.0	0.701(9)	O	1.0	0.01695
O4	0.3426(28)	0.2505(10)	0.788(6)	O	1.0	0.01695
O5	0.3455(27)	0.1336(12)	0.079(4)	O	1.0	0.01695
O6	0.3562(27)	0.1239(11)	0.597(4)	O	1.0	0.01695
O7	0.2636(31)	0.0	0.410(6)	O	1.0	0.01695
M1	0.0	0.0921(10)	0.5	Mg	0.125*	0.01109
M1	0.0	0.0921(10)	0.5	Fe^{2+}	0.59(2)	0.01109
M2	0.0	0.1814(6)	0.0	Fe^{3+}	1.0	0.01109
M3	0.0	0.0	0.0	Fe^{2+}	1.0	0.01109
M4	0.0	0.2808(15)	0.5	Na	0.83(4)	0.01967
Am	-0.013(11)	0.5	0.155(23)	Na+Ca	0.182(26)	0.01967

* = population fixed to the value from the chemical analysis; ** = an overall parameter for each chemical species was refined.

subtracted R_{wp} = 4.78% and R_p = 2.77%, χ^2 = 3.063 for 1573 observations, 255 reflections and 77 variables; (ii) peritoneum spleen crocidolite fibers: background subtracted R_{wp}= 2.77% and R_p = 1.97%, χ^2 = 0.526 for 947 observations, 289 reflections and 47 variables; (iii) peritoneum pancreas crocidolite fibers: background subtracted R_{wp} = 2.08% and R_p = 1.66%, χ^2 = 0.589 for 947 observations, 248 reflections and 48 variables. As an example, Figure 7 reports the graphical output of the refinement of raw crocidolite. The calculated structure parameters of raw crocidolite are reported in Table 1. The chemical composition of the sample calculated from the refinement is: $(Na,Ca)_{0.37}Na_{1.66}(Mg_{0.50}Fe^{2+}_{2.36}Fe^{3+}_{2})Si_8O_{22}(OH)_2$. With respect to the chemical composition reported by Kohyama et al. (1996), a slight overestimation of Na+Ca (2.03 against 1.77) is observed.

The calculated interatomic distances are reported in Table 2 whereas Table 3 illustrates the cation content of the raw crocidolite fibers and of those identified in the peritoneum surfaces of spleen and pancreas. The distribution of the iron atoms in the M1, M2 and M3 sites is compatible with the findings of Martra et al. (1999), who suggest that Fe^{2+} and Fe^{3+} are located in the three cases at fixed position and are not interchangeable one with other. The

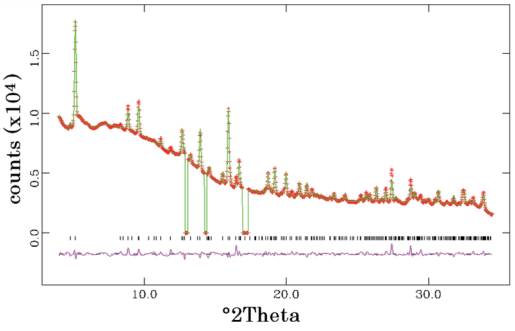

Figure 7. Graphical output of the refinement of raw crocidolite. Regions with peaks from the sample holder/environment were excluded.

Table 2. The interatomic distances calculated from the Rietveld refinement of raw crocidolite.

T1-O1 = 1.591(14)	M2-O1 = 2.186(27)	M4-O2 = 2.341(29)
T1-O5 = 1.652(13)	M2-O1 = 2.186(27)	M4-O2 = 2.341(29)
T1-O6 = 1.677(14)	M2-O2 = 1.941(27)	M4-O4 = 2.466(34)
T1-O7 = 1.681(12)	M2-O2 = 1.941(27)	M4-O4 = 2.466(34)
	M2-O4 = 2.074(23)	M4-O5 = 2.840(30)
T2-O2 = 1.594(13)	M2-O4 = 2.074(23)	M4-O5 = 2.840(30)
T2-O4 = 1.595(13)		M4-O6 = 2.343(31)
T2-O5 = 1.648(14)	M3-O1 = 2.284(26)	M4-O6 = 2.343(31)
T2-O6 = 1.689(13)	M3-O1 = 2.284(26)	
	M3-O1 = 2.284(26)	Am-O5 = 2.75(5)
M1-O1 = 2.090(27)	M3-O1 = 2.284(26)	Am-O5 = 2.75(5)
M1-O1 = 2.090(27)	M3-O-H3 = 2.09(4)	Am-O6 = 2.92(9)
M1-O2 = 2.062(27)	M3-O-H3 = 2.09(4)	Am-O6 = 2.92(9)
M1-O2 = 2.062(27)		Am-O7 = 2.958(23)
M1-O-H3 = 2.107(24)		Am-O7 = 3.06(14)
M1-O-H3 = 2.107(24)		Am-Am = 1.31(17)

calculated interatomic distances are very similar to those reported by Hawthorne (1978) for fluor-riebeckite, the only exception being the large M3-O mean distance (2.217 Å for our sample and 2.113 Å for the fluor-riebeckite). The shorter M-O mean distance found for the M2 site (2.068 Å for our sample and 2.027 Å for the fluor-riebeckite) may confirm the ordering of Fe^{3+} in that site.

Although the quality of these results is too poor to depict an indisputable model for the structure modification of the crocidolite fibers in organic media, some differences between the raw fibers and those inoculated in the peritoneum medium are detected. It is known from the literature (Crawford and Miller, 1981) that

Table 3. Cation site distribution in raw, pancreas and spleen crocidolites.

site	x/a	y/b	z/c	Cation	Occ. Raw crocidolite	Occ. *In situ* crocidolite in pancreas	Occ. *In situ* crocidolite in spleen	U_{iso}(Å^2)**
M1	0.0	0.0921(10)	0.5	Mg 0.125*	0.125*	0.125*	0.01109	
M1	0.0	0.0921(10)	0.5	Fe^{2+} 0.59(1)	0.77(3)	0.84(6)	0.01109	
M2	0.0	0.1814(6)	0.0	Fe^{3+}	1.0	0.92(6)	0.82(11)	0.01109
M3	0.0	0.0	0.0	Fe^{2+}	1.0	1.0	1.0	0.01109
M4	0.0	0.2808(15)	0.5	Na	0.83(4)	0.94(8)	0.92(8)	0.01967
Am	-0.013(11)	0.5	0.155(23)	Na+Ca	0.182(26)	0.09(5)	0.10(5)	0.01967

Legend: * = population fixed to the value from the chemical analysis; ** = an overall parameter for each chemical species was refined.

crocidolite in lung tissues shows reduced crystallinity due to erosion associated with the (100) planar defects and surface dissolution. The latter is likely a result of the leaching of Mg atoms, leaving a silicate skeleton, in an analogous manner to the mechanism proposed for chrysotile (Morgan et al., 1977). Although it is not possible to confirm the microstructure models proposed in the literature, for which a dedicated TEM study is mandatory, an indirect evidence of reduced crystallinity comes from the calculated values of the profile broadening coefficients. A lower crystallinity is expected for the pancreas and spleen crocidolites as, on equal values of Lx (1.07, 1.3 and 1.22 for spleen, pancreas and raw crocidolite, respectively), their GW values are notably larger (29.0 and 28.4, respectively) with respect to that of the raw sample (22.9). The pH of the peritoneum chemical environment, hosting the crocidolite fibers in the pancreas and spleen tissues, is 6.1-6.3. Such acidic environment prompts solubility of Fe^{2+} (whereas Fe^{3+} is not soluble) and may be the chemical gradient promoting the dissolution of the crocidolite fibers. The mobilization of iron from crocidolite phagocytised by cultured human lung carcinoma cells, even at higher pH values (6.8), has already been reported by Chao et al. (1994).

In fibers identified both at spleen and at pancreas peritoneal surface, intra-structure diffusion is apparently observed, with iron migrating from site M2 to site M1 and sodium migrating from site Am to site M4 (Figure 8). Cation redistribution is not surprising in crocidolite in contact with acidic solutions such as water-base solution of ferric salts used for detoxification (see for example Hearne et al., 1993). On the other hand, it is not possible to assess whether iron migrated in site M1 is Fe^{3+} or the reduced species Fe^{2+}. In fact, the limited quality of the collected data does not permit the refinement of the position of M sites for the pancreas and spleen crocidolite, preventing the opportunity to detect the distribution of Fe^{2+}/Fe^{3+} in the crystallographic sites by the analysis of interatomic distances. As a matter of fact, it is also possible that iron migration from site M2 to site M1 actually counter-balances a migration of Mg from site M1 to site M2. In any case, the redistribution of positive charges seems to call for a counter-balance migration of sodium (and eventually calcium). According to Pascolo et al. (2013), cation mobilization is the first step of interaction of asbestos fibers with tissues: Fe^{2+} is oxidized to Fe^{3+} and migrates outside the structure to form ferrihydrate-rich ferritin and hematite, calcium and magnesium migrate to prompt phagocytosis induced calcification. For the reasons explained above, this model needs further confirmation and the basic chemical factor that promotes this ion migration is still unclear. To accomplish a robust and sound general model of the crocidolite fiber modification and dissolution mode in organic media and unequivocally understand the mechanism of the fiber-cell interaction at a molecular level, it is necessary to further investigate their structures possibly using a X-ray microfocus (coupled, when available, with micro-Raman) at a synchrotron source. Gunter et al. (2011) recently performed such an analysis using synchrotron radiation to show different Fe oxidation states of asbestiform and non-asbestiform amphiboles from the same deposit.

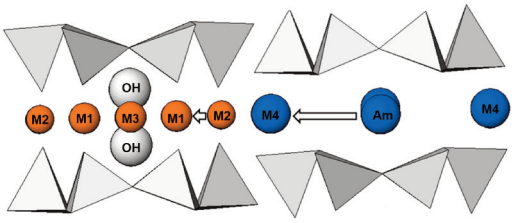

Figure 8. Crocidolite structure calculated from the Rietveld refinements showing iron migration from site M2 to site M1 and sodium migration from site Am to site M4 observed in fibres found in both pancreas and spleen peritoneum.

Conclusions

Crocidolite fibers injected in mice peritoneum were studied by micro-Raman and in situ synchrotron diffraction to contribute to the understanding of the MM developed by this mineral fibers. The identification of fibers in the different sections performed by means of an optical microscope allowed to reckon crocidolite fibers in the peritoneum lining spleen and pancreas. The fibers occurred free or coated by ferro-protein aggregates, which form around asbestos fibers to constitute the well-known "asbestos bodies". Our attention was focused on changes in the chemical or structural characteristics of the crocidolite fibers in contact with the biological medium. The main result obtained from the micro-Raman spectroscopy experiments was that on the spectra from crocidolite fibers in mice tissue sections, the Raman bands produced by the vibrations of the tetrahedral part of the crystalline structure -Si-O bonds- do not show sensible shifts or broadening, but only reduction in intensity. On the contrary in the spectral region containing the vibrational modes of the cubic and octahedral components of the crystalline structure, the bands appear less intense, eventually broadened and constituted by more components, or shifted with respect to the wavenumbers of the same bands in raw crocidolite. These results may be indicative of a partial degradation of the crystalline structure when the fibers reside in the biological matrix. This hypothesis is confirmed by X-ray diffraction study. In the analysed tissues, intra-structure diffusion is observed, with iron migrating from site M2 to site M1 although it is not possible to assess whether intra-structural iron oxidation occurs. The cation mobilization seems to regard sodium and possibly calcium too, in agreement with the picture drawn by Pascolo et al. (2013) who postulate cation mobilization as the first step of interaction of asbestos fibers with tissues.

On the same experimental trace marked out by Pascolo et al. (2011, 2013), the use of a microfocus synchrotron X-ray beam, coupled with Raman spectroscopy, is required to characterize single crocidolite fiber incorporated in mice and confirm the preliminary picture of the structure model of crocidolite in contact with the biological medium. The structure/microstructure features of each fiber should be correlated with its spectroscopic behaviour obtaining more detailed information about the change of the crystal structure and relation with Raman bands ascribed to different polyhedra.

Acknowledgements

The authors wish to thank the European Synchrotron Radiation Facility for provision of synchrotron radiation facilities (project HS-4422, BM01A), we would like to thank Volodymir Svitlyk for assistance in using beamline and M.E. Gunter for the revision of the manuscript. The authors also wish to thank the second anonymous referee and the editors for their work.

Animal experiments were supported by the Hawaii Community Foundation (to H.Y. and to G.G.), by NCI P01 CA 1140047 and Butitta Mesothelioma Foundation (to M.C.).

References

Apopei A.I. and Buzgar N. (2010) - The Raman study of amphiboles. *Analele Ştiinţifice Ale Universităţii Al. I. Cuza" Iaşi,* Seria Geologie, Tomul LVI, 57-83.

Arul K.J. and Holt P.F. (1980) - Clearance of asbestos bodies from the lung: a personal view. *British Journal of Industrial Medicine*, 37, 273-277.

Aust A.E., Cook P.M. and Dodson R.F. (2011) - Morphological and chemical mechanisms of elongated mineral particle toxicities. *Journal of Toxicology and Environmental Health, Part B: Critical Reviews*, 14, 40-75.

Bard D., Yarwood J. and Tylee B. (1997) - Asbestos fiber identification by Raman microspectroscopy.

Journal of Raman Spectroscopy, 28, 803-809.

Bernstein D., Castranova V., Donaldson K., Fubini B., Hadley J., Hesterberg T., Kane A., Lai D., McConnell E.E., Muhle H., Oberdorster G., Olin S. and Warheit D.B. (2005) - Testing of fibrous particles: short-term assays and strategies. Report of an ILSI Risk Science Institute Working Group. *Inhalation Toxicology*, 17, 497-537.

Bowes D.R. and Farrow C.M. (1997) - Major and trace element compositions of the UICC standard asbestos samples. *American Journal of Industrial Medicine*, 32, 592-594.

Brody A.R. (1993) - Asbestos-induced lung disease. *Environmental Health Perspectives*, 100, 21-30.

Burns R.G. and Prentice F.J. (1968) - Distribution of iron cations in the crocidolite structure. *The American Mineralogist*, 53, 770-776.

Carbone M., Ly B.H., Dodson R.F., Pagano I., Morris P.T., Dogan A.U., Gazdar A.F., Pass H.I. and Yang H. (2012) - Malignant mesothelioma: facts, myths, and hypotheses. *Journal of Cellular Physiology*, 277, 44-58.

Case B.W., Abraham J.L., Meeker G., Pooley F.D. and Pinkerton K.E. (2011) - Applying definitions of "asbestos" to environmental and "low-dose" exposure levels and health effects, particularly malignant mesothelioma. *Journal of Toxicology and Environmental Health, Part B: Critical Reviews*, 14, 3-39.

Chao C.C., Lund L.G., Zinn K.R. and Aust A.E. (1994) - Iron mobilization from crocidolite asbestos by human carcinoma cells. *Archives of Biochemistry and Biophysics*, 314(2), 384-391.

Cole R.W., Ault J.G., Hayden J.H. and Rieder C.L. (1991) - Crocidolite asbestos fibers undergo size-dependent microtubule-mediated transport after endocytosis in vertebrate lung epithelial cells. *Cancer Research*, 51, 4942-4947.

Crawford D. and Miller K. (1981) - Structure and structural changes in crocidolite asbestos associated with biological systems. *Micron*, 12, 25-28.

Croce A., Musa M., Allegrina M., Rinaudo C., Baris Y.I., Dogan A.U., Powers A., Rivera Z., Bertino P., Yang H., Gaudino G. and Carbone M. (2013a) - Micro-Raman spectroscopy identifies crocidolite and erionite fibers in tissue sections. *Journal of Raman Spectroscopy*, early view.

Croce A., Musa M., Allegrina M., Trivero P. and Rinaudo C. (2013b) - Environmental scanning electron microscopy technique to identify asbestos phases inside ferruginous bodies. *Microscopy and Microanalysis*, 19, 420-424.

De Vuyst P., Dumortier P. and Gevenois P.A. (1997) - Analysis of asbestos bodies in BAL from subjects with particular exposures. *American Journal of Industrial Medicine*, 31, 699-704.

Dodson R.F., O'Sullivan M., Corn C.J., Garcia J.G.N., Stocks J.M. and Griffith D.E. (1993) - Analysis of ferruginous bodies in bronchoalveolar lavage from foundry workers. *British Journal of Industrial Medicine*, 50, 1032-1038.

Foresti E., Fornero E., Lesci I.G., Rinaudo C., Zuccheri T. and Roveri N. (2009) - Asbestos health hazard: a spectroscopic study of synthetic geoinspired Fe-doped chrysotile. *Journal of Hazardous Materials*, 167, 1070-1079.

Fornero E., Allegrina M., Rinaudo C., Mazziotti-Tagliani S. and Gianfagna A. (2008) - Micro-Raman spectroscopy applied on oriented crystals of fluoro-edenite amphibole. *Periodico di Mineralogia*, 77, 5-14.

Fubini B. and Mollo L. (1995) - Role of iron in the reactivity of mineral fibers. *Toxicology Letters*, 82/83, 951-960.

Gellert A.R., Kitajewska J.Y., Uthayakumar S., Kirkham J.B. and Rudd R.M. (1986) - Asbestos fibers in bronchoalveolar lavage fluid from asbestos workers: examination by electron microscopy. *British Journal of Industrial Medicine*, 43, 170-176.

Ghio A.J., Churg A. and Roggli V.L. (2004) - Ferruginous bodies: implications in the mechanism of fiber and particle toxicity. *Toxicologic Pathology*, 32, 643-649.

Giacobbe C., Gualtieri A.F., Quartieri S., Rinaudo C., Allegrina M. and Andreozzi G. (2010) - Spectroscopic study of the product of thermal transformation on chrysotile-asbestos containing materials (ACM). *European Journal of Mineralgy*, 22, 535-546.

Goodglick L.A. and Kane A.B. (1990) - Cytotoxicity of long and short crocidolite asbestos fibers in vitro and in vivo. *Cancer Research*, 50, 5153-5163.

Gunter M.E., Dyar M.D., Lanzirotti A., Tucker J.M. and Speicher E.A. (2011) - Differences in Fe-Redox for asbestiform and nonasbestiform amphiboles from the former vermiculite mine, near Libby, Montana USA. *American Mineralogist*, 96, 1414-1417.

Guthrie G.D. Jr (1992) - Biological effects of inhaled

minerals. *American Mineralogist*, 77, 225-243.

Hammersley J. (1996) - FIT2D User manual. ESRF publication, Grenoble, France.

Hawthorne F.C. (1978) - The crystal chemistry of the amphiboles. VIII. The crystal structure and site chemistry of fluor-riebeckite. *Canadian Mineralogist*, 16, 187-194.

Hearne G.R., Kolk B., Pollak H., van Wyk J.A. and Gulumian M. (1993) - Bulk and surface modifications in detoxified crocidolite. *Journal of Inorganic Biochemistry*, 50, 145-156.

Huang S.X.L., Jaurand M.C., Kamp D.W., Whysner J. and Hei T.K. (2011) - Role of mutagenicity in mineral fiber-induced carcinogenicity and other diseases. *Journal of Toxicology and Environmental Health, Part B: Critical Reviews*, 14, 179-245.

Koerten H.K., Hazekamp J., Kroon M. and Daems W.Th. (1990) - Asbestos body formation and iron accumulation in mouse peritoneal granulomas after the introduction of crocidolite asbestos fibers. *American Journal of Pathology*, 136, 141-157.

Kohyama N., Shinohara Y. and Suzuki Y. (1996) - Mineral phases and some reexamined characteristics of the International Union Against Cancer asbestos samples. *American Journal of Industrial Medicine*, 30, 515-528.

Langer A.M., Rubin I.B. and Selikoff I.J. (1972) - Chemical characterization of asbestos body cores by electron microprobe analysis. *Journal of Histochemistry & Cytochemistry*, 20, 723-734.

Larson A.C. and Von Dreele R.B. (1994) - Generalized Structure Analysis System, Los Alamos Nat. Lab., New Mexico, LAUR, 86-748.

Lewis I.R., Chaffin N.C., Gunther M.E. and Griffiths P.R. (1996)- Vibrational spectroscopic studies of asbestos and comparison of suitability for remote analysis. *Spectrochimica Acta Part A*, 52, 315-328.

Martra G., Chiardola E., Coluccia S., Marchese L., Tomatis M., and Fubini B. (1999) - Reactive sites at the surface of crocidolite asbestos. *Langmuir*, 15, 5742-5752.

Mastrangelo G., Marangi G., Ballarin M.N., Michilin S., Fabricio A.S.C., Valentini F., Lange J.H., Fedeli U., Cegolon L. and Gion M. (2011) - Osteopontin, asbestos exposure and pleural plaques: a cross-sectional study. *BMC Public Health*, 11, 220-227.

Morgan A., Davies P., Wagner J.C., Berry G. and Holmes A. (1977) - The biological effects of magnesium-leached chrysotile asbestos. *The British Journal of Experimental Pathology*, 58, 465-473.

Mossman B., Light W. and Wei E. (1983) - Asbestos: mechanisms of toxicity and carcinogenicity in the respiratory tract. *Annual Review of Pharmacology and Toxicology*, 23, 595-615.

Musa M., Croce A., Allegrina M., Rinaudo C., Belluso E., Bellis D., Toffalorio F. and Veronesi G. (2012) - The use of Raman spectroscopy to identify inorganic phases in iatrogenic pathological lesions of patients with malignant pleural mesothelioma. *Vibrational Spectroscopy*, 61, 66-71.

Pascolo L., Gianoncelli A., Kaulich B., Rizzardi C., Schneider M., Bottin C., Polentarutti M., Kiskinova M., Longoni A. and Melato M. (2011) - Synchrotron soft X-ray imaging and fluorescence microscopy reveal features of asbestos body morphology and composition in human lung tissues. *Particle and Fiber Toxicology*, 8, 7.

Pascolo L., Gianoncelli A., Schneider G., Salomé M., Schneider M., Calligaro C., Kiskinova M., Melato M. and Rizzardi C. (2013) - The interaction of asbestos and iron in lung tissue revealed by synchrotron based scanning X-ray microscopy. *Scientific Reports*, 3(1123), 1-11.

Rihn B., Coulais C., Kauffer E., Bottin M.C., Martin P., Yvon F., Vigneron J.C., Binet S., Monhoven N., Steiblen G. and Keith G. (2000) - Inhaled crocidolite mutagenicity in lung DNA. *Environmental Health Perspectives*, 108, 341-346.

Rinaudo C., Allegrina M., Fornero E., Musa M., Croce A. and Bellis D. (2010a) - Micro-Raman spectroscopy and VP-SEM/EDS applied to the identification of mineral particles and fibers in histological sections. *Journal of Raman Spectroscopy*, 41(1), 27-32.

Rinaudo C., Belluso E. and Gastaldi D. (2004) - Assessment of the use of Raman spectroscopy for the determination of amphibole asbestos. *Mineralogical Magazine*, 68(3), 455- 465.

Rinaudo C., Croce A., Musa M., Fornero E., Allegrina M., Trivero P., Bellis D., Sferch D., Toffalorio F., Veronesi G. and Pelosi G. (2010b) - Study of inorganic particles, fibers, and asbestos bodies by variable pressure scanning electron microscopy with annexed Energy dispersive spectroscopy and micro-Raman spectroscopy in thin sections of lung and pleural plaque. *Applied Spectroscopy*, 64(6), 571-577.

Rinaudo C., Gastaldi D. and Belluso E. (2003) -

Characterization of chrysotile, antigorite and lizardite by FT-Raman spectroscopy. *Canadian Mineralogist*, 41, 883-890.

Rinaudo C., Gastaldi D., Belluso E. and Capella S. (2005) – Application of Raman spectroscopy on asbestos fiber identification. *Neues Jahrbuch für Mineralogie*, 182(1), 31-36.

Sakai Y., Ohbayashi C., Itami H., Kajimoto K, Sakuma T., Uchino K., Yoshimura M., Matsumoto S., Idei Y. and Oka T. (2010) - Simple quantitative analysis of asbestos body using the sediment of formalin injected into surgically resected lung cancers. *Pathology International*, 60, 78-86.

Tannapfel A. (2011) - Malignant Mesothelioma. Bochum, Germany, Springer Verlag.

Toby B.H. (2001) - EXPGUI, a graphical user interface for GSAS. *Journal of Applied Crystallography*, 34, 210-213.

Toyokuni S. (2009) - Mechanisms of asbestos-induced carcinogenesis. *Nagoya Journal of Medical Science*, 71, 1-10.

Wagner J.C., Griffiths D.M. and Hill R.J. (1984) - The effect of fiber size on the in vivo activity of UICC crocidolite. *British Journal of Cancer*, 49, 453-458.

Werner A.J., Hochella M.F. Jr, Guthrie G.D. Jr, Hardy J.A., Aust A.E. and Rimstidt J.D. (1995) - Asbestiform riebeckite (crocidolite) dissolution in the presence of Fe chelators. Implications for mineral-induced diseases. *American Mineralogist*, 80, 1093-1103.

Yang H., Rivera Z., Jube S., Nasu M., Bertino P., Goparaju C., Franzoso G., Lotze M.T., Krausz T., Pass H.I., Bianchi M.E. and Carbone M. (2010) - Programmed necrosis induced by asbestos in human mesothelial cells causes high-mobility group box 1 protein release and resultant inflammation. *Proceedings of the National Academy of Sciences of the United States of America*, 107, 12611-12616.

Yao S., Della Ventura G. and Petibois C. (2010) - Analytical characterization of cell-asbestos fiber interactions in lung pathogenesis. *Analytical and Bioanalytical Chemistry*, 397, 2079-2089.

Zucali P.A., Ceresoli G.L., De Vincenzo F., Simonelli M., Lorenzi E., Gianoncelli L. and Santoro A. (2011) - Advances in the biology of malignant pleural mesothelioma. *Cancer Treatment Reviews*, 37, 543-558.

Submitted, February 2013 - Accepted, June 2013